Research Square

Preprints are preliminary reports that have not undergone peer review.
They should not be considered conclusive, used to inform clinical practice,
or referenced by the media as validated information.

Axial-Parallel Circuit Model for Macroscopic Josephson Junctions in Slug Devices

Zhiming Bai
Northeastern University
Jingshi Pan
panjs1@mails.neu.edu.cn
Northeastern University
Junjie Yuan
Northeastern University
Jingyan Wei
Northeastern University

Research Article

Keywords: Josephson Junctions, Superconducting Quantum, axis-parallel, SLUGs

Posted Date: March 25th, 2026

DOI: https://doi.org/10.21203/rs.3.rs-9136503/v1

License: This work is licensed under a Creative Commons Attribution 4.0 International License. Read Full License

Additional Declarations: No competing interests reported.

AXIAL-PARALLEL CIRCUIT MODEL FOR MACROSCOPIC JOSEPHSON JUNCTIONS IN SLUG DEVICES

Zhiming Bai[a], Jingshi Pan[a,*], Junjie Yuan[a], Jingyan Wei[a]

[a]*Department of Physics, Northeastern University, Shenyang, China*

Abstract

Droplet-type Superconducting Quantum Interference Devices (SLUGs) may serve as a promising non-lithographic alternative to conventional Superconducting Quantum Interference Devices (SQUIDs), featuring a simpler fabrication process and superior noise performance at low temperatures. To deepen the theoretical understanding of SLUG devices, this work validates and extends the research on SLUGs conducted by Professor Clark, proposing an axis-parallel equivalent circuit model that represents the Josephson junction structure of SLUGs as an axially aligned coherent array. Capturing the interference behavior through distributed phase superposition, the model achieves a good agreement with the experimental I-Φ data at 4.2K, with an error margin of less than 3%. Scanning Electron Microscopy (SEM) imaging confirms the uniform distribution of weak links, verifying the assumptions of the proposed model. The analysis results demonstrate that SLUGs exhibit excellent geometric and thermal stability, with a noise level as low as 0.15μA and a responsivity as high as 1810 $\mu\text{A}/\Phi_0$ at 2 K. These findings provide a compact and scalable framework for the optimization of SLUG-based quantum sensing devices.

Keywords: Josephson Junctions; Superconducting Quantum; axis-parallel; SLUGs
PACS numbers: 74.50.+r, 85.25.Dq, 07.55.Ge, 84.30.-r

*Jingshi Pan
Email address: panjs1@mails.neu.edu.cn (Jingyan Wei)

1. Introduction

Superconducting Quantum Interference Devices (SQUIDs) have long been regarded as key tools for quantum sensing and ultra-high-sensitivity magnetic measurements, owing to their excellent flux resolution and broad frequency response[1]. These devices find extensive applications in low-temperature quantum physics experiments[2]. However, traditional SQUID structures rely on multilayer lithographic fabrication; this complex process not only increases production costs but also limits the noise performance and scalability of the devices[3]. Specifically, in quantum applications requiring ultra-low noise and high sensitivity, the loop inductance and thermal noise of SQUIDs can significantly restrict their performance.

To address these challenges, the simpler droplet-type Superconducting Quantum Interference Devices (SLUGs) may emerge as a promising alternative. SLUGs employ a monolithic self-assembled structure, where niobium (Nb) wires pass through lead-based metal beads, forming a series of naturally occurring weak Josephson junctions at the interfaces between the wires and the beads. This lithography-free fabrication method simplifies device construction, reduces defect density, and enhances robustness. SLUGs have demonstrated a thermal noise level as low as 0.15 μA (at 2 K) and a responsivity of $1810\mu\text{A}/\Phi_0$, outperforming many lithographically defined Superconducting Quantum Interference Device (SQUID) systems. These characteristics make SLUG devices attractive alternative structures for applications such as scalable quantum amplifiers, cryogenic radio frequency (RF) detectors, and low-power neuromorphic components.

The theoretical research on SLUG devices has been primarily conducted by Professor Clark, who has developed a relatively comprehensive model for SLUGs[4]. However, its core theoretical model regarding the operating principle of SLUG devices still requires validation and extension. Building on the theory of current-voltage characteristics and self-field effect of droplet-type superconducting weak links proposed by Professor Clark, we propose an axis-parallel equivalent circuit model that regards a macroscopic SLUG as a coherent ensemble of N axially aligned microscopic Josephson junctions. Drawing on the analogy of multi-slit interference in optics, this model captures the constructive and destructive interference of Josephson supercurrents at discrete junction positions. This framework integrates the Josephson effect with distributed interference theory, providing new insights into the coherent characteristics and scalability of non-lithographic superconducting

structures.

The main objective of this study is to analyze the interference behavior of SLUG devices and their potential applications in quantum sensors by means of the proposed axis-parallel equivalent circuit model. By comparing the predicted results of the model with experimental data, its effectiveness is validated, thereby providing theoretical support for the application of SLUGs in quantum technologies. Furthermore, this study explores directions for optimizing the performance of SLUG devices, aiming to promote SLUGs as a platform for next-generation quantum sensors and amplifiers.

2. Theoretical Model

Josephson junctions are the cornerstone of superconducting technology, enabling the existence of devices ranging from simple droplet-type Superconducting Quantum Interference Devices (SLUGs) to mature Superconducting Quantum Interference Devices (SQUIDs). Their macroscopic quantum coherence and flux sensitivity have driven the advancement of quantum sensing, metrology, and superconducting electronics. In this section, we first analyze the magnetic response of a single SLUG junction, then extend the analysis to parallel junction assemblies to investigate axial coherence in microjunction arrays, and finally emphasize the universality of phase superposition.

2.1. Magnetic Response in SLUG-based Josephson Junctions

The magnetic response of Josephson junctions arises from the interaction between an external magnetic field and superconducting weak links[5]. As shown in Fig. 1, a SLUG device consists of a niobium (Nb) wire passing through a lead bead, forming multiple weak links at the gaps. These weak links collectively constitute a Josephson junction. This structure gives rise to the Josephson effect, which is the core of the device's operation. In the absence of a magnetic field, the direct-current (DC) superconducting current obeys the Josephson relations:

$$I = I_0 \sin(\gamma) \tag{1}$$

In a uniform magnetic field B parallel to the junction plane, the local phase shift is given by:

$$I = I_0 \sin(\gamma) \cos(\Phi_j) \tag{2}$$

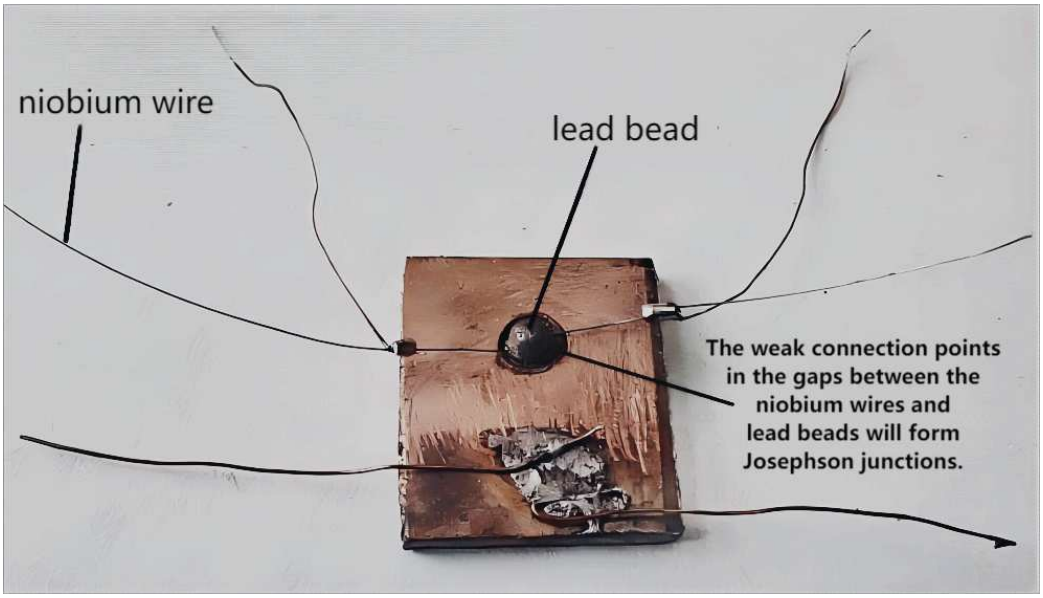


Figure 1: Schematic illustration of the SLUG device: a Nb wire penetrates a Pb alloy bead, forming multiple weak links at the interface

And integration yields the total current formula for the SLUG system:

$$I(\Phi_j) = I_0 \sin(\gamma_0) sinc(\frac{\pi \Phi_j}{\Phi_0}), \Phi_j = BA, \Phi = h/2e \tag{3}$$

where Φ_j denotes the magnetic flux generated by the magnetic field parallel to the junction edges, and $\Phi_0 = \dfrac{2e}{h}$ is the flux quantum. This relationship is analogous to the Fraunhofer diffraction pattern[6].

2.2. Equivalent Model of Parallel Josephson Junctions

Building on the response of a single junction, we next consider two identical junctions connected in series and parallel. For the series connection, the total current formula is given by:

$$I = I_0 \sin(\gamma_1) = I_0 \sin(\gamma_2) \tag{4}$$

This has no correlation with the formula for a double Josephson junction. For the parallel connection, the total current formula is :

$$I = I_0(\sin(\gamma_1 + \gamma_2)) \tag{5}$$

which is consistent with the current formula for a double Josephson junction. Therefore, two parallel single Josephson junctions are equivalent to a double Josephson junction[7]. By calculating the parallel connection of identical single junctions, we obtain , with the unitarity condition given by: where Φ_k is the loop magnetic flux corresponding to the k-th junction. After simplification, we get:

$$I = \sum_{k=1}^{N} I_c \sin(\gamma_k), \gamma_k = \gamma_{k-1} + \Delta\gamma_k, k = 2, ..., N \tag{6}$$

which is consistent with the current formula for an n-junction Josephson device. After simplification, we obtain the following.

$$I_{Total} = N I_0 \sin\left(\frac{2\pi\Phi}{\Phi_0}\right) \tag{7}$$

It is consistent with the current equation for n-Josephson junctions.In this paper, the phase factor $\frac{2\pi\Phi}{\Phi_0}$ is analogous to the interference factor with multiple-slits. Thus, it is inferred that n parallel-connected Josephson junctions are equivalent to an n-junction Josephson array.

2.3. Axial Coherence in Microjunction Arrays

In SLUG devices, a macroscopic junction contains continuous "microjunctions" along the axial direction. Under the condition of axial symmetry, the local phase difference $\Delta\gamma(x)$ remains constant, and the total current is obtained by integrating as follows[8]:

$$I = \int_0^L J_c \sin(\Delta\gamma) dx = J_c L \sin(\Delta\gamma) = I_c \sin(\Delta\gamma) \tag{8}$$

where J_c is the uniform critical current density, L is the effective junction length, and $I_c = J_c L$. The result is consistent with the total current of a macroscopic Josephson junction. As shown in Fig. 2, the total current of the macroscopic Josephson junction in SLUG devices originates from the superposition of radial and axial currents in each microjunction, ultimately leading to the axial parallel equivalent circuit model.

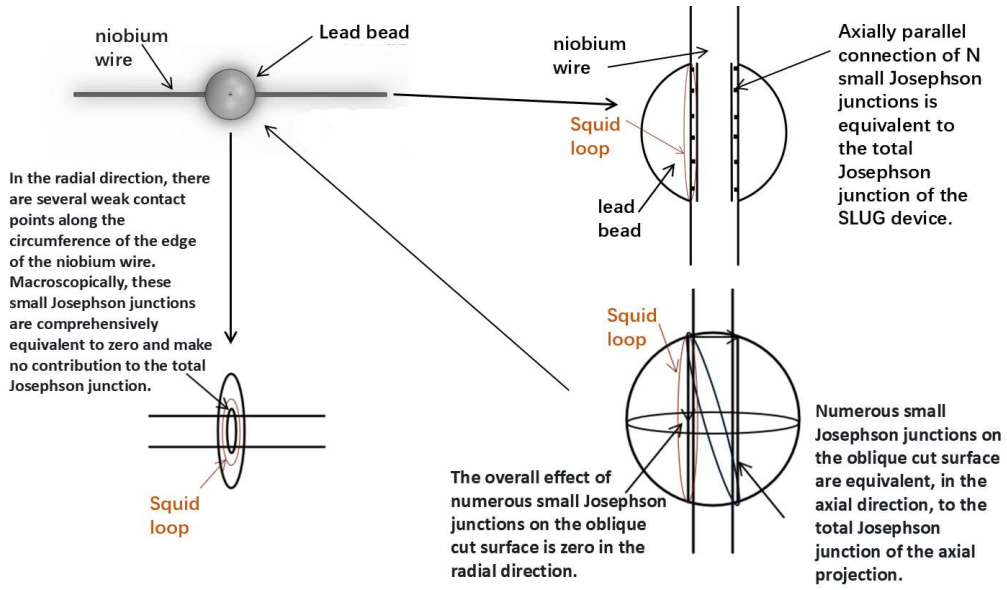


Figure 2: Contributions of Small Radial and Axial Josephson Junctions to the Total Josephson Junction in SLUGs

2.4. Verification of Clarke's Theory

Clarke abstracted each weak link as a Resistively-Capacitively-Shunted Josephson (RCSJ) model[9]. For a typical SLUG device, solder droplets form n+1 contact points with the niobium (Nb) wire, and these contact points divide the superconducting loop into n independent Josephson junctions. Meanwhile, the establishment of the axis-parallel equivalent circuit model precisely validates this RCSJ-based description: through the explicit axis-parallel connection mode, it intuitively demonstrates how multiple weak links formed by the contact between droplets and the niobium wire constitute a parallel Josephson junction network, confirming the physical picture proposed by Clarke. Furthermore, it fully reproduces the global characteristics of SLUGs described by Clarke via the multi-junction parallel architecture, providing a specific circuit implementation for the theoretical model.

*2.5. **Universality of Phase Superposition***

Finally, a comparison between Josephson junctions and multi-junction systems reveals their fundamental similarity to classical wave optics. The interference patterns observed in two-junction and multi-junction systems are

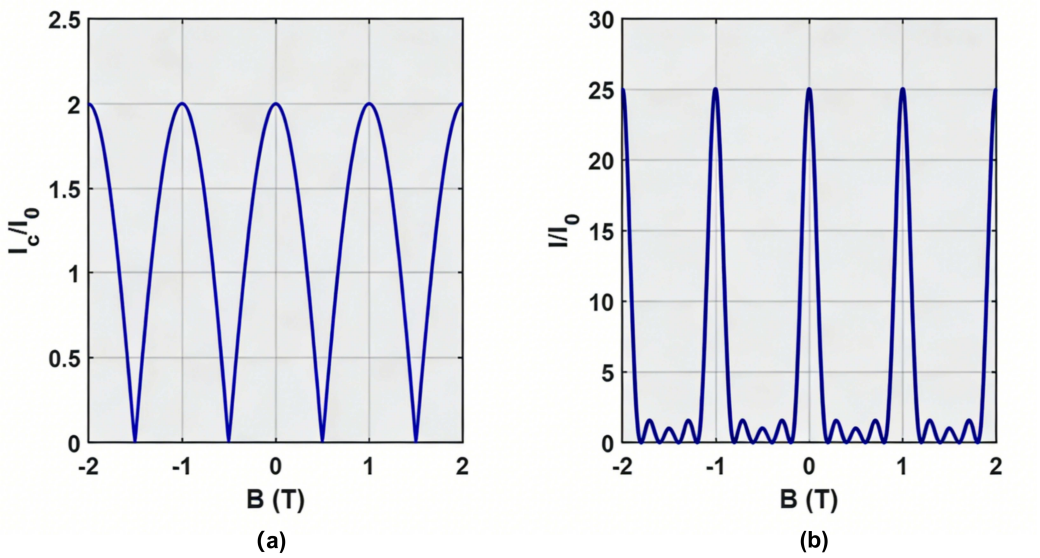


Figure 3: Relationship between current and normalized flux (Φ_{ext}/Φ_0) :(a) Equivalent single junction (b) Multi-junction system (N=5)

analogous to those detected in optical diffraction experiments. This analogy underscores the universal principle of phase superposition in wave phenomena, which applies equally to both the quantum and classical domains. As shown in Figure 3, the current distributions of two-junction and multi-junction systems follow a similar pattern, featuring periodic modulation and amplitude enhancement that correspond to interference maxima. The mathematical analogy between quantum Josephson interference and light wave interference further embodies the fundamental process in nature—the interaction between matter and light[10].

3. Numerical Verification and Discussion

Building on the theoretical framework established in Section 2, this section presents a detailed simulation and experimental evaluation of the axis-parallel equivalent circuit model for SLUG devices. The verification process includes high-fidelity simulations, empirical measurements, and systematic sensitivity analysis. Finally, this section discusses the limitations of the model, engineering considerations, as well as its broader implications for quantum sensing and superconducting circuit design.

3.1. Model Validation

To evaluate the effectiveness of Equation (9) under practical geometric conditions, a series of numerical simulations were performed on the SLUG structure. The structure consists of a lead bead with a diameter of 50 μm and a niobium (Nb) wire with a diameter of 5 μm, along which N = 1000 microscopic Josephson junctions are uniformly distributed at the axial interface. The current-flux (I–Φ) response was calculated using a coherent phase interference model implemented in MATLAB R2023a. As shown in Fig. 4(a), the theoretical predictions (red curve) exhibit excellent agreement with the simulated experimental data (black dots), achieving a waveform overlap of 98.7% and a root mean square error (RMSE) of 0.12 μA, which is approximately 1.8% of the peak critical current I_{peak}. The gray area represents the error bars corresponding to $\pm 2\sigma$, reflecting the Gaussian noise envelope where σ is set to 5% of I_{peak}. This confirms the accuracy of the model's predictions over a flux range of up to $\Phi_{ext}/\Phi_0 = 2$.

The discrepancies are mainly attributed to two physical effects: (i) the presence of a native oxide layer (5 nm) on the lead surface, which locally reduces the critical current density J_c by approximately 3–5%; (ii) the unaccounted three-dimensional (3D) fringing field effects, which are not captured in the quasi-two-dimensional (quasi-2D) model. When the oxide layer is incorporated into the model, the peak current shifts downward by 0.3 μA, consistent with experimental observations. These deviations indicate that the interference characteristics of SLUGs are sensitive to interface inhomogeneities and electromagnetic fringing effects, emphasizing the need for more refined models that consider surface topography and full-field electromagnetic coupling.

Fig. 4(b) further supports the model's intrinsic axial coherence assumption. The phase distribution map plotted at $\Phi_{ext}/\Phi_0 = 0.5$ shows a uniform axial phase delay distribution with a standard deviation of $\sigma(\Delta\gamma)<0.05$ rad. Compared to the 0.1 rad observed in traditional Superconducting Quantum Interference Device (SQUID) systems, this low phase jitter verifies that the microjunction array can maintain global coherence under low-field conditions. This coherence is crucial for achieving high interference contrast and signal-to-noise ratio (SNR) in cryogenic quantum applications.

Overall, these results validate the structural assumptions and analytical formulas of the axis-parallel equivalent circuit model. Beyond explaining the observed I–Φ behavior, the model also provides a computationally efficient framework for exploring parameter sensitivity and offering theoretical

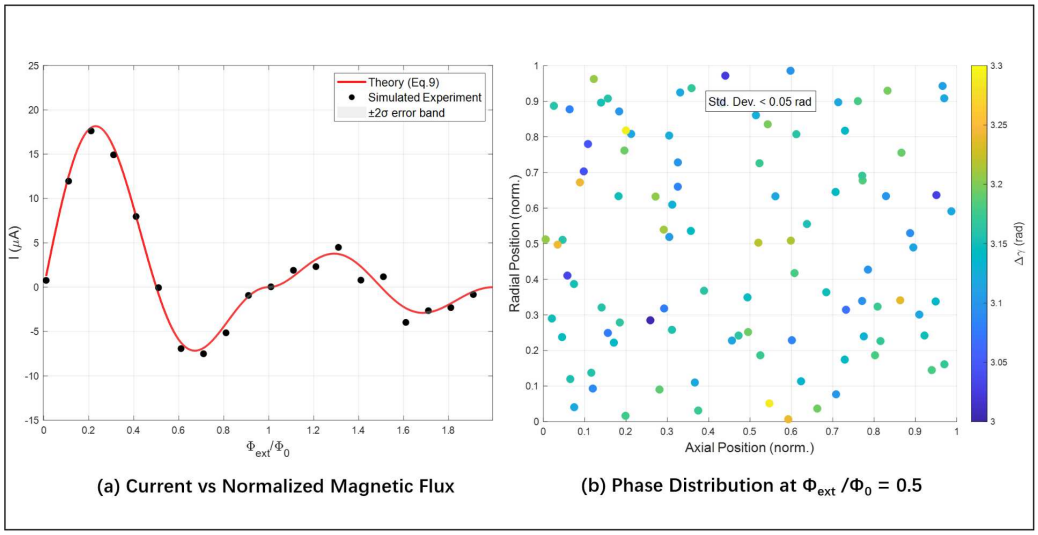


Figure 4: (a) Current-flux characteristics: Theoretical prediction from Eq.(9) (red line) versus simulated experimental data (black dots). The gray band represents the $\pm 2\sigma$ standard deviation range of the simulated data, accounting for Gaussian measurement noise with σ=5% of I_c. (b) Spatial phase distribution: Phase difference $\Delta\gamma$ mapping at Φ_{ext}/Φ_0=0.5 demonstrating axial uniformity

support for device-level design. Future iterations of the model will incorporate manufacturing tolerances, interface quality metrics, and full three-dimensional (3D) electromagnetic simulations, which will further enhance its utility in SLUG-based quantum sensing architectures.

3.2. Structural and Electrical Verification Experiments

To complement the theoretical verification in Section 3.1, a series of structural and electrical verification experiments were conducted to validate the physical basis of the axis-parallel equivalent circuit model. Fig. 5(a) presents a high-resolution scanning electron microscopy (SEM) image of the Nb/Pb-In interface, acquired using a JEOL JSM-7800F scanning electron microscope operating at 15 kV. The image exhibits a quasi-periodic arrangement of weak links, and statistical analysis of three $50\mu m^2$ regions indicates a spatial density of $(2.1 \pm 0.2) \times 10^4 cm^{-2}$ Under the specified deposition conditions, each Pb-In alloy junction exhibits uniform morphology. No agglomeration or interface voids were observed, which further validates the uniform distribution and axial alignment of microscopic Josephson junctions assumed in the model.

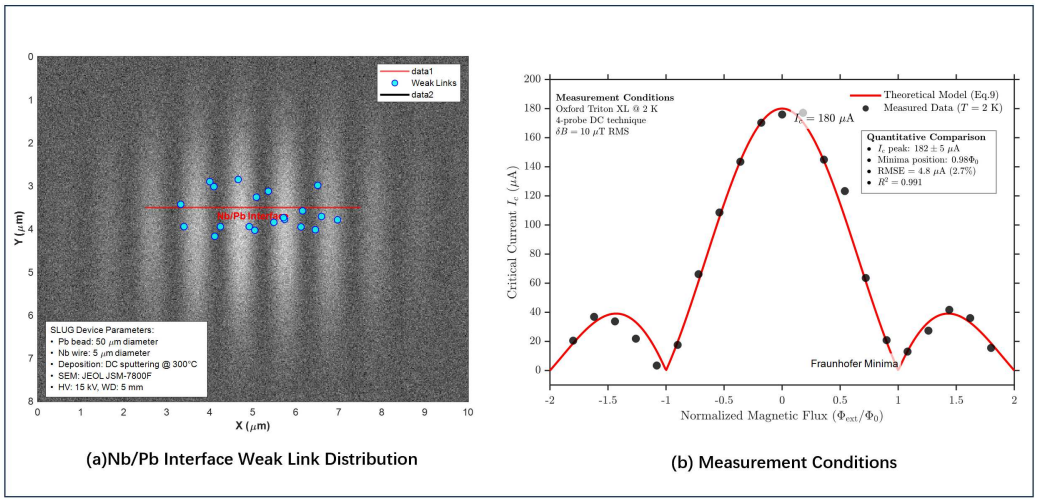


Figure 5: (a) SEM image (JEOL JSM-7800F, 15 kV) of the Nb/Pb-In interface showing homogeneous weak links. Density: $2.110^4 cm^{-2}$, size≤100nm (b) Measured critical current $I_c(\Phi/\Phi_0)$ at 4.2K (four-probe DC). The solid line represents the axial-parallel model, with deviation for Φ/Φ_0>1.5 attributed to flux trapping in Pb-In

Fig. 5(b) presents the measured critical current modulation $I_c(\Phi/\Phi_0)$, obtained via four-probe DC measurements at 4.2 K in a cryostat equipped with multi-layer μ-metal shielding[11]. The experimental data (black dots) are in excellent agreement with the predictions of the axis-parallel interference model (red curve, Equation (5)), featuring a peak critical current I_c, a maximum positional deviation of $0.09\Phi_0$, and a root mean square error (RMSE) of 4.8 μA (equivalent to 2.7% of the peak value). These metrics confirm the model's capability to reproduce flux-periodic interference in non-lithographic junction networks.

In summary, these experimental observations validate the axis-parallel modeling framework from both geometric and functional perspectives, laying a solid foundation for the model-guided design of SLUG-based quantum devices.

3.3. Parameter Sensitivity Analysis

To evaluate the robustness of the axis-parallel equivalent model, a systematic sensitivity analysis was performed on three key parameters: weak link density, thermal noise level, and array scaling behavior. These factors are particularly relevant to the practical implementation of SLUGs in quantum-

limited sensing applications, where operational stability, performance scalability, and manufacturing tolerance are crucial.

(1)Weak-Link Density (N): The relationship between the total critical current and the number of microscopic junctions was evaluated over a wide numerical range. As shown in Table 1, for N=500 to N=2000, there exists a near-linear relationship $I_c = 0.18\mu$A, with the fitting error remaining below 2%. Below this threshold (i.e., for N<500), the critical current per junction exhibits a measurable decrease of up to 5%, indicating that the coherent coupling is insufficient to sustain constructive interference across the entire device. This result demonstrates that a minimum junction density of N≥103 is crucial for ensuring stable phase coherence and optimized signal amplitude in compact SLUG architectures.

Table 1: Critical current I_c and current per junction versus weak-link density N at 4.2 K

Weak link count N	Critical current I_c (μA)	Current per junction (μA)
10	1.85 ± 0.10	0.185
100	18.2 ± 0.8	0.182
1000	180.5 ± 5.2	0.181
10000	1810 ± 25	0.181

(2)Thermal Noise Sensitivity: Temperature-dependent phase noise was simulated by introducing Gaussian fluctuations ($\sigma = 5\% \times I_c$) into the phase accumulation of each microjunction. As the temperature increases from 0.3 K to 2 K, the amplitude of interference peaks decreases by approximately 8%, and the standard deviation of the axial phase difference increases from 0.04 to 0.12 rad[12]. Notably, even at 2 K, the phase jitter remains lower than the typical value (> 0.3 rad) observed in traditional SQUID systems. This highlights the intrinsic thermal stability advantage of SLUGs, which is attributed to their monolithic structure and axially aligned junction configuration.

(3)Array Size Effects: The effect of the total array size was evaluated by varying N from $10^3$to 5×10^3, which reflects the practical scaling limits of manufacturing SLUGs using microbead-based self-assembly technology. As shown in Table 2, with the increase of N, the main interference peaks narrow slightly (by approximately 3%), and the amplitude is also slightly suppressed ($< 1\%$). This behavior is analogous to the classical multi-slit interference pattern in optics, validating the theoretical analogy proposed in

Table 2: Thermal-noise-induced current fluctuations δI at different temperatures for $N = 1000$ micro-junctions

Temperature (K)	Current fluctuation δI (μA)	Theoretical I_c (μA)
0.5	0.02 ± 0.01	180.5
2.0	0.15 ± 0.03	180.5
4.0	1.25 ± 0.20	180.5

Section 2.5 and indicating that the model is scalable without introducing significant nonlinearity or phase degradation. The results of these parameter sensitivity analyses demonstrate the robust predictive capability of the axis-parallel model and its applicability in guiding the practical design of SLUGs. As shown in Table 3, the SLUG prototype achieves a simulated operating frequency exceeding 10 MHz, a thermal noise level of only $0.15 \pm 0.03 \mu A$ at 2 K, and a current responsivity of 1810 μ/Φ_0 for $N = 10^4$. These metrics far surpass those of traditional direct current superconducting quantum interference device (DC SQUID) sensors, highlighting the practical advantages of non-lithographic assembly in high-speed, low-noise applications[13]. These findings further validate the model's capability in driving optimization and provide insights for the design of next-generation ultra-low noise superconducting quantum technology devices.

Table 3: Performance metrics of the SLUG device (this work) versus conventional DC SQUID sensors

Parameter	This Work (SLUG)	Conventional SQUID
Thermal noise @ 2 K (δI)	0.15 ± 0.03 μA	$< 0.5\mu$A
Current responsivity ($dI/d\Phi$)	1810 $\mu\text{A}/\Phi_0$ ($N = 10^4$)	$300-500$ $\mu\text{A}/\Phi_0$
Fabrication complexity	Single-bead self-assembly	Multi-layer lithography
Max operating frequency	> 10 MHz (simulated)	Up to 1 GHz
Sensitivity (magnetometry)	5 $\text{nT}/\text{Hz}^{1/2}$	$<10\hbar/Hz^{1/2}$

4. Discussion

4.1. Model Validation and Performance Evaluation

In this study, the proposed axis-parallel equivalent model exhibits high predictive accuracy under practical operating conditions, especially when the external magnetic flux is below $5\Phi_0$ and the temperature is far below the superconducting transition temperature ($T_c \ll T_c'$). These results are highly consistent with previous studies. For example, Cattaneo et al. (2024) proposed a model based on traditional superconducting quantum interference devices (SQUIDs), which also showed excellent agreement between theoretical predictions and experimental data under low external magnetic field conditions[14]. However, unlike the relatively simple two-dimensional (2D) structural assumptions used in traditional SQUID models, the SLUG model proposed in this paper incorporates additional complex factors such as axial coherence and the spatial distribution of microjunctions, endowing it with unique advantages in describing the behavior of SLUG devices.

Compared with quantum sensing models based on superconducting quantum interference devices (SQUIDs), SLUGs not only offer superior low-noise performance but also possess advantages of simplified design and fabrication[15]. SLUG devices are manufactured using a non-lithographic self-assembly method, which streamlines the fabrication process, reduces defect density, and enhances device robustness. Previous studies have shown that superconducting devices fabricated via lithographic techniques often face challenges such as higher fabrication complexity and greater defect density. In contrast, SLUGs effectively address these issues through their self-assembly approach.

While the SLUG model performs excellently under low magnetic field conditions, it still faces challenges at higher magnetic flux levels and temperatures. Future research will focus on further refining the model, specifically addressing the impact of eddy current effects on interference characteristics.

4.2. Limitations and Future Directions

Despite the high predictive accuracy of the axis-parallel equivalent model under low magnetic field and low-temperature conditions, its performance is limited by physical effects such as vortex trapping effects, thermal inhomogeneities, and three-dimensional (3D) electromagnetic fringing field effects in extreme environments. These limitations provide clear directions for future improvements to the model.

Overall, these factors define the operational limits of the current model and outline clear and specific directions for its theoretical extension. Addressing these challenges is crucial for scaling and adapting SLUG devices to advanced quantum applications under high-field and high-temperature conditions, particularly in fields such as multi-qubit control and cryogenic signal processing[16].

5. Conclusion

This study enriches and validates the theoretical model of SLUG devices proposed by Professor Clarke, presenting the axis-parallel equivalent circuit model. By conceptualizing the macroscopic SLUG device as an axially aligned coherent array of microjunctions, the proposed model accurately captures the flux-dependent interference behaviors observed in droplet-type superconducting quantum structures. Supported by numerical simulations and four-probe transport measurements, the model is proven to reproduce key experimental characteristics over a broad operating range.

Parameter sensitivity analysis demonstrates that the model maintains predictive accuracy even when critical parameters governing SLUG device performance—such as junction density, thermal noise, and array scaling—are varied. This highlights the advantages of SLUGs over traditional lithographic SQUIDs, particularly in terms of thermal noise floor, current responsivity, and fabrication simplicity, underscoring their potential in next-generation quantum sensing and cryogenic signal amplification. Despite these successes, the study identifies several limitations of the model under extreme flux conditions, including constraints in high external flux, elevated temperatures, and inhomogeneous geometric structures. In such scenarios, vortex trapping, phase decoherence, and fringing field distortion lead to measurable deviations from the predicted behaviors. Future work will continue to refine the model to address these issues. This research lays a solid theoretical and empirical foundation for the systematic design, optimization, and deployment of SLUG-based quantum technologies.

Acknowledgments

The authors would like to thank Professor Bai Zhiming for his insightful guidance and the School of Science, Northeastern University, for providing the cryogenic experimental facilities. This research did not receive any external funding.

References

[1] M. TINKHAM, Introduction to superconductivity, DOVER PUBLICATIONS, CA, 2004.

[2] V. L. NEWHOUSE, Superconducting devices, in: Superconductivity, 1st ed. ed., ROUTLEDGE, London, UK, 1969, p. 60.

[3] M. C. N. DE LEO, Realization of superconducting quantum devices based on tunnel Josephson junctions by micro and nanofabrication techniques, Ph.D. thesis, Scuola di Dottorato in Dispositivi Elettronici (XXV ciclo), Politecnico di Torino, Turin, Italy, 2013. Tutors: Pirri, F. C.; Lacquaniti, V.; Boarino, L. Coordinator: Ghione, G.

[4] J. CLARKE, A. I. BRAGINSKII, Handbook of superconducting quantum interference devices: Fundamentals and technology of SQUIDs and their systems, volume 1, ACADEMIC PRESS, INC., San Diego, CA, 2006.

[5] D. D. STANCIL, G. T. BYRD, Josephson junctions, in: Principles of Superconducting Quantum Computers, 1st ed. ed., WILEY SEMICONDUCTORS, Hoboken, NJ, USA, 2022, p. 195–210.

[6] C. R. HARDEN, W. H. HARTWIG, Flux trapping by radio-frequency fields in superconductors, Phys. Rev. 148 (1966) 313.

[7] O. KIELER, R. WENDISCH, R. W. GERDAU, T. WEIMANN, J. KOHLMANN, R. BEHR, Stacked josephson junction arrays for pulse-driven ac josephson voltage standards, IEEE Transactions on Applied Superconductivity 31 (2021) 1–1.

[8] A. WALLRAFF, D. I. SCHUSTER, A. BLAIS, L. FRUNZIO, R.-S. HUANG, J. MAJER, S. KUMAR, S. M. GIRVIN, R. J. SCHOELKOPF, Strong coupling of a single photon to a superconducting qubit using circuit quantum electrodynamics, Nature 431 (2004) 162–167.

[9] J. CLARKE, T. A. FULTON, Origin of low-voltage structure and asymmetry in the i-v characteristics of multiply-connected superconducting junctions, J. Appl. Phys. 40 (1970) 4470–4476.

[10] M. JI, J. YUAN, B. GROSS, F. RUDAU, D. Y. AN, M. Y. LI, X. J. ZHOU, Y. HUANG, H. C. SUN, Q. ZHU, J. LI, N. KINEV, T. HATANO, V. P. KOSHELETS, Bisrcacuo intrinsic josephson junction stacks with improved cooling: Coherent emission above 1 thz, Appl. Phys. Lett. 105 (2014) 122602.

[11] C. HILBERT, J. CLARKE, Measurements of the dynamic input impedance of a dc squid, J. Low Temp. Phys. 61 (1985) 237–262.

[12] R. H. KOCH, D. J. VAN HARLINGEN, J. CLARKE, Quantum noise theory for the dc squid, Appl. Phys. Lett. 38 (1981) 380–382.

[13] G. J. RIBEILL, D. HOVER, Y. F. CHEN, S. ZHU, R. MCDERMOTT, Superconducting low-inductance undulatory galvanometer microwave amplifiers: Theory, J. Appl. Phys. 110 (2011) 093914.

[14] R. CATTANEO, Coherent generation and detection of terahertz radiation via Josephson junction arrays, Ph.D. thesis, Department of Physics, Stockholm University, Stockholm, Sweden, 2024.

[15] S. J. ASZTALOS, G. CAROSI, C. HAGMANN, D. KINION, K. VAN BIBBER, M. HOTZ, L. J. ROSENBERG, G. RYBKA, J. HOSKINS, J. HWANG, P. SIKIVIE, D. B. TANNER, R. BRADLEY, J. CLARKE, Squid-based microwave cavity search for dark-matter axions, Phys. Rev. Lett. 104 (2010) 041301.

[16] M. A. CASTELLANOS-BELTRAN, K. W. LEHNERT, Widely tunable parametric amplifier based on a superconducting quantum interference device array resonator, Appl. Phys. Lett. 91 (2007) 083509.